Molecular-dynamics simulations of picosecond pulsed laser ablation and desorption of silicon

Patrick Lorazo,[a,b] Laurent J. Lewis,[b] Michel Meunier[a]

[a]Département de Génie Physique et de Génie des Matériaux et Groupe de Recherche en Physique et Technologie des Couches Minces (GCM), École Polytechnique de Montréal, Case Postale 6079, Succursale Centre-Ville, Montréal, Québec, Canada, H3C 3A7

[b]Département de Physique et Groupe de Recherche en Physique et Technologie des Couches Minces (GCM), Université de Montréal, Case Postale 6128, Succursale Centre-Ville, Montréal, Québec, Canada H3C 3J7

ABSTRACT

Molecular-dynamics simulations are used to investigate single-shot pulsed laser ablation and desorption of crystalline silicon. The motion of approximately 32000 atoms, contained in a $5 \times 5 \times 27$ nm^3 surface rectangular box irradiated by a single 308 nm, 10 ps, Gaussian laser pulse is followed on the picosecond time scale. Because melting and, possibly, ablation or desorption of the target following absorption of the laser pulse are described within the thermal annealing model, care is taken not to exceed carrier densities of $\sim 10^{22}$ cm^{-3}. More precisely, the interaction of photons with the target is thought to cause the generation of a dense gas of hot electrons and holes which thermalises, at first, on a time scale of a few tens of femtoseconds through carrier-carrier scattering. These hot photocarriers then transfer their kinetic energy to the lattice by means of carrier-phonon interactions characterized by a very fast initial cooling rate. The result is the creation, above a characteristic threshold energy, of a plume containing single atoms and clusters leaving the target with high axial velocities. Preliminary results about the melting fluence threshold and mechanisms underlying ablation are presented. Carrier diffusion is found to be an essential mechanism for relaxation and is presented as a possible cause of subsurface boiling.

Keywords: Laser ablation, desorption, thermal annealing model, molecular dynamics, carrier diffusion, plume, silicon

1. INTRODUCTION

Laser ablation,[1-3] the removal of atoms, ions, clusters, molecules and electrons upon the interaction of a laser pulse with a target of a given material, has been used for many years already for various purposes including controlled removal of tissue in surgery as well as micromachining, microsurgery, surface cleaning and pulsed laser deposition (PLD) of thin films[4] in microelectronics. Despite the extensive use of laser beams for microstructuring surfaces, a complete picture of the numerous mechanisms leading to ablation is still lacking.

At the same time, increasingly powerful computers have allowed the limits of computational techniques to be pushed further and further. Among them, molecular dynamics (MD) has been used to study various systems on the microscopic scale, even allowing, more recently, the properties of new materials which either have not yet been investigated or remain to this day inaccessible to experiment to be predicted. As a matter of fact, the MD technique which provides the motion of atoms in real time when the interatomic forces are known, appears particularly suitable for the study of laser ablation, as it involves many different phenomena; no hypothesis about the latter are needed, only the interatomic potential having to be defined. However, as pointed out by Zhigilei et al.,[5] the *collective* nature of the phenomenon, as well as the relatively long time scale, hamper the study of laser ablation through brute force MD simulations; thus there have been very few attempts[5-8] until now. In order to elude these difficulties, Zhigilei et al. have developed a breathing-sphere model[5,9,10] for the MD simulations of laser ablation and desorption of organic solids, where each molecule is represented as a sphere possessing a single internal degree of freedom, sufficient to account for its vibrational relaxation in a realistic manner. These simulations have allowed to define more precisely the underlying microscopic mechanisms:[9] the laser-induced pressure build-up and the phase

---

Further author information: E-mail: lorazop@magellan.umontreal.ca

explosion due to overheating appear to be the key processes determining the dynamics of laser ablation. Interestingly, a well-defined fluence threshold[10] separates *desorption*, a regime resulting essentially in the ejection of single particles following sublimation or vaporization, from ablation, a collective phenomenon leading to a high proportion of clusters in the plume.

MD simulations, together with the Stillinger-Weber potential (SW),[11] have also recently been used to study the laser ablation of silicon,[6] with the aim of understanding the micromachining of silicon surfaces with ultrashort femtosecond laser pulses, as well as the influence of such parameters as the width and fluence of the pulse on the dimensions of the hole created by the ablative process. However, the predicted ablation thresholds were found to be at least an order of magnitude higher than the corresponding experimental values.[12,13] A possible reason for this discrepancy could be related to the choice of the interatomic potential: a critical carrier density $n_c \sim 10^{22}$ cm^{-3} is believed[14,15] to be separating two distinct regimes and, for lower carrier concentrations, *thermal processes only* are operative; at carrier densities exceeding n_c, melting proceeds as an ultrafast process in 1 ps or less following the absorption of the laser pulse. The former regime, described by the thermal annealing model (TAM), is observed with nanosecond and picosecond pulses, while the latter is particular to ultrashort laser pulses, typically of 100 fs or less. Thus, while the SW potential provides a convenient and satisfying way to recreate the interactions among the silicon atoms in both solid and liquid phases *when thermal processes are involved*, there are good reasons to believe that it is not suitable to describe an ultrafast melting process such as the the one that can be observed with femtosecond pulses.

In the present paper, we propose a model for the interaction of 308 nm (4.03 eV) picosecond laser pulses with a crystalline silicon target. Silicon has been chosen for its importance in the microelectronics industry and because it is reasonably well described by the SW potential. However, as noted above, this restricts us to situations involving only thermal processes (i.e. within TAM) and, consequently, to pulses not shorter than 10 ps[16] and fluences leading to carrier densities lower than 10^{22} cm^{-3}. More specifically, we are interested in delineating the various mechanisms that lead to ablation and possibly see if it is possible to establish a common trend among various materials based on recent simulations.[9] Moreover, we wish to determine if a distinct fluence threshold, separating desorption from ablation, can be observed for silicon and what is the resulting composition of the plume. Finally, thermal ablation (following thermal melting) being a phenomenon occurring typically on a 10^{-10} s time scale,[14] the use of ultrashort laser pulses (femto- and pico-) allows us to avoid the difficulty of considering the interaction of the pulse with the ejected particles. The simulation of laser ablation and desorption in the picosecond regime therefore offers great challenges, numerous questions remaining to be answered.

2. THE MODEL

2.1. Target and Laser Pulse

We are first concerned with the description of the target and the laser pulse *before* they interact with each other.

2.1.1. The target

Because of computational limitations, the supercell is restricted to a total of 32400 atoms in a box of approximately $5 \times 5 \times 27$ nm^3, of which about 28000 are forming a (100) *surface* slab of $5 \times 5 \times 24$ nm^3 that is exposed to the laser pulse. The latter box is chosen to represent a small portion of the target *at the center of the laser pulse*.

In order to recreate the thermal and structural constraints of a macroscopic crystal, the supercell is first replicated to infinity in the x and y directions, that is to say parallel to the upper surface, through the use of periodic boundary conditions. Along the z axis though, thermalization is ensured by coupling the system to a heat reservoir; in practice, this is done by renormalizing the velocities of a few layers of atoms at the bottom of the supercell to an appropriate Maxwell-Boltzmann (MB) distribution. Additionally, a layer of atoms, attached to their equilibrium position through a spring at 300 K, is placed below the heat reservoir in order to mimic a semi-infinite crystal in the z direction. The latter layer forms, together with the heat reservoir and the previously mentioned surface slab, the supercell.

2.1.2. The laser pulse

For a 10 ps laser pulse, which is Gaussian in time as well as in the lateral directions, and of macroscopic width, because the simulation box width is spanning a relatively small scale (a few nanometers), any spatial variation of the irradiance can be considered negligible. When periodic boundary conditions are imposed along the x and y axis, the irradiance is thus, in effect, spatially *constant* over the infinite xy plane. However, the supercell being located in

the center of the laser pulse, the perturbation induced by a constant irradiance far from the region under study can be ignored.

The large number of photons contained in each pulse, typically a few tens of thousands, ensures a uniform spatial distribution of the energy in the xy plane. The temporal Gaussian distribution can be simulated by a succession of planes spanning the entire top surface of the supercell, each containing a well defined number of photons corresponding to the instantaneous irradiance and separated in time by an interval ranging from Δt to typically $10 \times \Delta t$, where $\Delta t = 0.5$ fs is the value of the MD timestep.

2.2. Absorption of Light

At $\lambda = 308$ nm, each photon has an energy of 4.03 eV, larger than the Si bandgap energy of 1.12 eV at 300 K.[17] There are three possible absorption mechanisms: (1) an interband transition following the absorption of a single photon by a valence electron, through which the latter is promoted to the conduction band and a hole is left behind; (2) a non-linear, multiphoton, interband transition following the simultaneous absorption of two or more photons by a single valence electron that can possibly lead to its photoemission; (3) an intraband transition, or free-carrier absorption, according to which the photon is absorbed by an electron already in the conduction band.

The rate of generation of carriers by the laser pulse can be written as

$$G = \frac{(1 - \Gamma)\alpha I(z,t)}{h\nu} + \frac{(1 - \Gamma)^2 \beta I^2(z,t)}{2h\nu} , \tag{1}$$

$(1 - \Gamma)I(z,t)$ being the intensity of the laser at a depth z below the surface of the target, Γ the reflection coefficient at the surface, α the one-photon interband absorption coefficient, and β the two-photon interband absorption coefficient. It is instructive to compare the two-photon and one-photon generation rates, that is the ratio

$$\frac{G_2}{G_1} = (1 - \Gamma)I(z,t)(\frac{\beta}{2\alpha}) . \tag{2}$$

At $\lambda = 308$ nm and 300 K, $\Gamma \sim 0.60$,[16] $\alpha \sim 1.5 \times 10^6$ cm^{-1},[16] and $\beta \sim 40$ cm/GW;[18] with an irradiance as high as 10^3 GW/cm^2, which is at least an order of magnitude higher than the ones we consider in this work, equation (2) gives $\frac{G_2}{G_1} \leq 0.01$. Thus, we expect one-photon interband transitions to be at least a 100 times more frequent than two-photon interband transitions. Moreover, it has been shown[19] that free-carrier absorption is negligible at short wavelengths, typically below 1000 nm. Therefore, in the present simulations, the one-photon interband transition is the dominant mechanism for absorption and all other mechanisms are ignored.

When a photon reaches the surface of the target, its position (x_i, y_i) in the xy plane is determined through a uniform probability distribution, and is reflected or not according to the temperature-dependent reflection coefficient of silicon, which was obtained from a fit of experimental data.[20] If not reflected, the photon is assumed to be absorbed according to the Beer-Lambert law, i.e. at a depth

$$z_i = -\alpha^{-1}\ln(\xi) \text{ cm} , \tag{3}$$

where ξ is a random number taken from a uniform distribution. A temperature-dependent relationship for the absorption coefficient α is used.[21] Once the location (x_i, y_i, z_i) of the absorption process has been determined, the silicon atom with at least one valence electron which lies closest is excited, i.e. its number of valence electrons decremented by one.

The absorption of a photon leads to the creation of an electron-hole pair. The position of the atom to which the electron belongs is taken as the initial position of the electron-hole pair. The latter then diffuses into the bulk as a result of the carrier concentration gradient (see section 2.3.3). For simplicity, the electron and the hole thus generated are assumed to move together at all times, that is to say a *single* coordinate is used to follow the pair; the Coulombian interaction between the carriers and with the ions and atoms are, thus, ignored.

The determination of the initial kinetic energy of each carrier would require the knowledge of the various optical transitions allowed. In order to elude this difficulty, it is reasonable, because the very fast carrier-carrier interactions lead to a Fermi-Dirac (FD) distribution at a temperature T_e within a few tens of femtoseconds, to assume an *instantaneous* quasi-equilibrium state of the electronic gas described by such a distribution. Because T_e is relatively

large, typically up to 10000 K, the FD distribution is approximated by a MB distribution. Thus, as an electron is excited into the conduction band and added to the existing electronic plasma, its initial kinetic energy is calculated according to the MB distribution at the current temperature T_e. If E_{K_i} is its initial kinetic energy, the hole then receives a kinetic energy equal to $(h\nu - E_G - E_{K_i})$. A carrier density and lattice temperature-dependent relationship is used for the bandgap energy E_G[22,23] of silicon.

Finally, the relatively large absorption coefficient at $\lambda = 308$ nm, combined with a depth of 24 nm for the simulation box, ensures that close to 98% of the energy is absorbed within the supercell.

2.3. Relaxation Processes

Following the generation of the electron-hole plasma, a number of processes allow the system to relax.

2.3.1. Carrier-phonon scattering

According to TAM, the energy transfer from the energetic carriers to the lattice proceeds via the scattering with phonons, mainly optical, within typically 1 ps. The latter then scatter with acoustic phonons, allowing the redistribution of the energy among all lattice modes within ~ 10 ps. The lattice is then in a state of quasi-equilibrium characterized by a Bose-Einstein distribution at temperature T.

It is possible to get a general picture of the various phonons emitted, as well as the rate at which they scatter with the carriers. There are many mechanisms for carrier-phonon scattering. Among them, the dominant mechanism for energetic *electrons* are the so-called *intervalley scattering transitions*, which imply large changes in momentum and thus phonons with wave vectors near the zone boundary.[24]

Generally, the probability per unit time S_{if} that a carrier with crystal momentum **p** scatters to a state with crystal momentum **p'** is given by[24]

$$S_{if} \propto D_{if}^2 , \tag{4}$$

where D_{if}, the intervalley deformation potential, characterizes the strength of the scattering from the initial valley i to the final valley f. From the various values of D_{if},[25] it is possible to evaluate the probability P_{if}, proportional to S_{if}, for each intervalley transition to occur. We find that almost 70% of phonons that scatter with electrons are optical. For holes, though, the main scattering mechanism[24] is *optical deformation potential scattering*; we thus assume the holes to scatter only with optical phonons of 62.6 meV. Finally, because the carriers are energetic, it is reasonable to assume that they are being scattered by phonons through, mainly, an emission process. Absorption of phonons is therefore negligible compared to spontaneous emission at all carrier energies.

The scattering processes having been identified, along with their probabilities, the scattering rate remains to be determined. A simple approach consists in using results[25] for the carrier-phonon scattering rate in silicon calculated using the full band-structure of the material. A polynomial fit of the curves for both electrons and holes at 300 K was done. In doing so, we elaborated an approximate but simple tool to estimate the phonon emission rate as a function of the carrier energy. Fluctuations of the scattering rates with temperature and bandgap energy are neglected. However, screening effects by carriers are incorporated in the way suggested by Yoffa,[26] where the critical carrier density for significant screening effects is taken to be equal to 1.2×10^{21} cm^{-3}.

Thus, the carriers can be viewed as virtual centers for the emission of phonons moving downward into the bulk. As they diffuse, the knowledge of their energy allows the rate at which they scatter with phonons to be calculated. This information is then used to determine, on the basis of a uniform probability distribution, the moment a phonon is emitted. The phonon energy is distributed instantaneously, according to a spatial Gaussian distribution, among all atoms in a radius of 5 Å around the scattered carrier. Once the phonon has been emitted, the carrier energy is updated. Moreover, the rate of scattering of a given carrier with phonons is updated every timestep as it depends on the *local* carrier density.

2.3.2. Other processes

Impact ionization, the process through which an electron-hole pair is created when a very energetic electron collides with a valence electron, can be safely neglected. Indeed, the generation of highly energetic carriers originating most probably from multiphoton interband transitions, and the latter absorption mechanism being negligible in the present context, impact ionization can be ignored.

Furthermore, in silicon, the dominant recombination mechanism is Auger.[27] It has been shown[28] that the recombination time, due to screening effects by the carriers, tends asymptotically toward a minimum value of 6 ps. As mentioned in section 2.3.3, because of the existence of a carrier density gradient near the surface, carriers diffuse into the bulk. However, because they generally diffuse out of the supercell in a characteristic time of less than 6 ps, Auger recombination can be neglected here. For relatively deeper simulation boxes, this simplification may not be valid.

2.3.3. Carrier diffusion

Carriers diffuse into the bulk as a result of the carrier density gradient, which is a direct consequence of the exponentially decreasing form of the absorption law with depth. Carrier diffusion is taken into account by using the relations suggested by Berz et al.[29] for the various components of the electron and hole mobilities. Each electron-hole pair is given an ambipolar diffusion coefficient that is updated every timestep in order to take into account the changes in the *local* carrier density and temperature. For simplicity, carrier diffusion is occurring along the z axis only and downward into the bulk as the carrier density gradient is assumed to be oriented in the latter direction.

3. RESULTS AND DISCUSSION

We give, in this section, preliminary results (i.e. the first few picoseconds) for the absorption of 308 nm, 10 ps, laser pulses with a crystalline silicon target. Two situations are analyzed. First, simulations for a single 0.16 J/cm^2 pulse are used to estimate the melting fluence. Second, simulations for a single 0.30 J/cm^2 pulse for which carrier diffusion has been suppressed are carried out to recreate artificial conditions where ablation occurs; mechanisms underlying ablation are studied and the resulting plume analyzed. The role of carrier diffusion within the relaxation process is discussed.

3.1. Melting Fluence

First, the melting fluence can be estimated and, along with other data, used to confirm the validity of the model. As an example, Fig. 1 shows, for a single 0.16 J/cm^2 pulse and a maximum surface irradiance of $\sim 4 \times 10^{10}$ W/cm^2 after 5 ps, the lattice-averaged temperature T and the surface temperature T_s. The laser pulse starts at t = 0 ps. Following the very fast initial relaxation of carriers, the lattice temperature averaged over the entire supercell reaches, before the end of the pulse, a plateau around $T \sim 2400$ K; when averaged over the top 7 nm, corresponding to the optical skin depth at $\lambda = 308$ nm, the temperature reaches a *lower* value of $T_s \sim 1800$ K. Thus, the surface temperature has reached the melting temperature ($T_m = 1685$ K for silicon), while the temperature *beneath* the surface is clearly
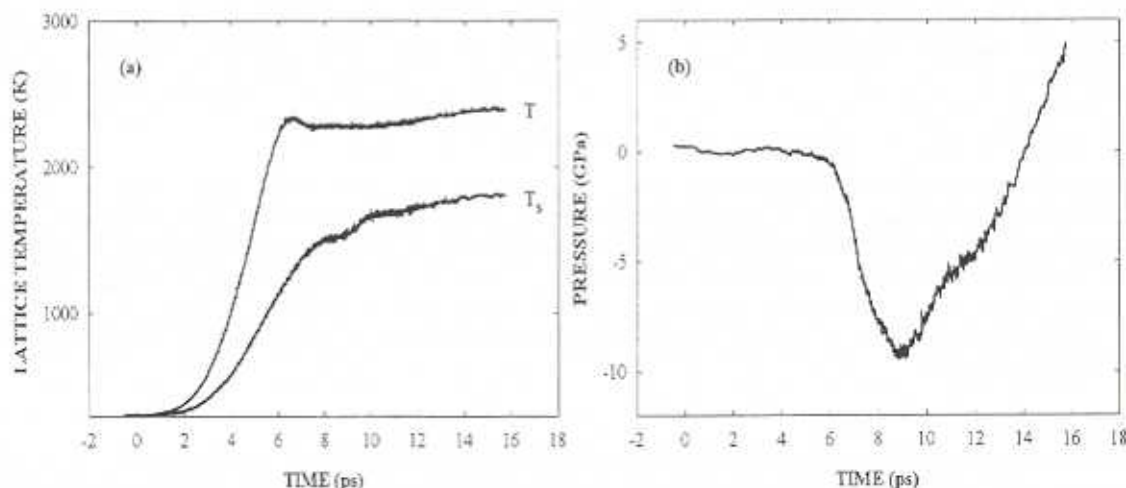

Figure 1. (a) Lattice average (T) and surface (T_s) temperatures vs time. (b) Average pressure vs time. Results are for a single 0.16 J/cm^2 laser pulse.

higher than T_s, a result of the carrier ambipolar diffusion. Even if, as a consequence of the exponentially-decaying absorption law, more carriers are generated near the surface, most of the energy is released beneath it due to the fact that electron-hole pairs diffuse into the bulk. This observation could possibly be related to the well-known phenomenon of *subsurface boiling*[4] which occurs when the time required to transform laser energy into heat is shorter than that needed to evaporate a surface layer of a thickness of the order of the skin depth. In the present case, melting has not yet occurred, as it takes roughly 50 to 100 ps to bring to a molten state a 20 nm surface layer of silicon using a picosecond laser pulse.[31] Nevertheless, we would expect, as the system evolves, to observe superheating and possibly subsurface boiling. The latter, sometimes referred to as "true splashing", can result in micron-sized molten globules to be expelled from the surface. Although the supercell is of nanometer size, further calculations on a longer time scale are needed to study such mechanisms.

Finally, it is possible to compare the predicted melting fluence threshold with experimental data; this is defined as the fluence required to bring the surface temperature to the bulk melting temperature. For instance, with a 100 fs, 632 nm laser pulse, von der Linde et al.[12] have determined the melting fluence threshold for a (100) silicon surface to be 0.15 J/cm² when melting is still occurring through thermal processes. For picosecond pulses, the melting threshold at $\lambda = 0.53$ μm was measured to be 0.2 J/cm².[32] These measurements are consistent with our observation of a surface temperature of $\sim$ 1800 K at 0.16 J/cm², suggesting a melting threshold around 0.15 J/cm².

3.2. Mechanisms of laser ablation and carrier diffusion

As can be seen in Fig. 1 for a 0.16 J/cm² pulse, the absolute value for the pressure (averaged over the entire supercell), initially very low, increases relatively fast once the laser pulse has begun: because a large amount of energy is stored in a very short time, the material does not have the possibility to undergo thermal expansion and a high pressure builds up within the volume. The pressure is negative, indicating tensile forces, and reaches an absolute value of $\sim$ 10 GPa after approximately 8.5 ps. This value is in good agreement with pressures deduced from experiment.[33]

Fig. 2 shows the evolution in time of the average coordination number at the surface at the same laser fluence. The average value of approximately 3.88, calculated for a 10 Å thick layer at the surface, is *not* related to the formation of an amorphous state but, rather, is a consequence of including in the calculation undercoordinated surface atoms. As will be discussed further below, the average coordination number can be used to signal a possible phase transition. Thus, as one can see, there is the creation of a high tensile pressure but there in no indication yet of a phase transition. Fig. 2 also shows, along the z axis, in box units, the position of the topmost layer as a function of time, which rises for the first 8.5 ps as a result of the tensile pressure build-up. The original upper limit of the supercell was set to zero. At this energy, ablation is not expected to occur.
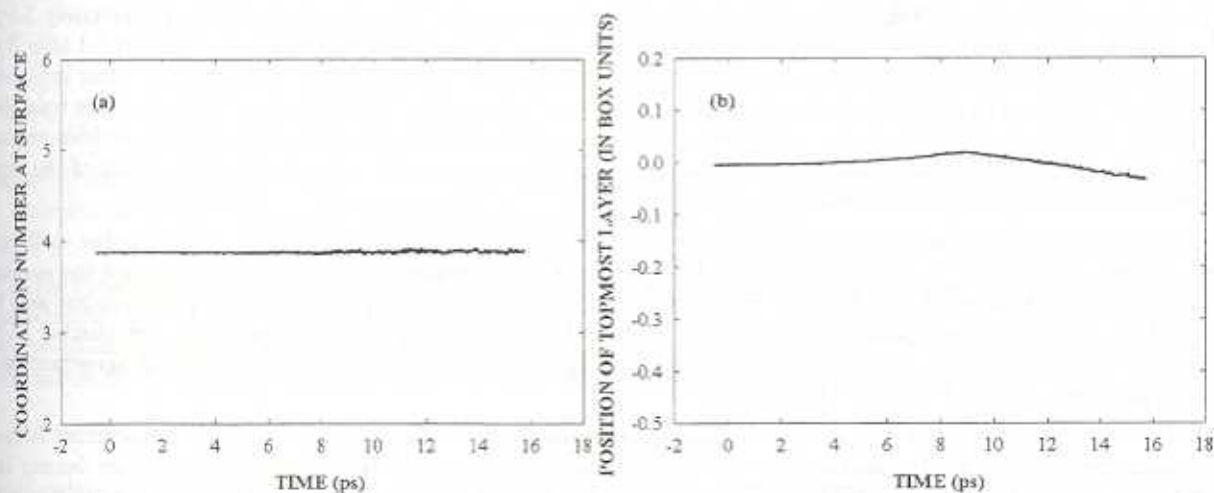

Figure 2. (a) Average coordination number at surface vs time. (b) Position of the surface layer vs time. Results are for a single 0.16 J/cm² laser pulse.
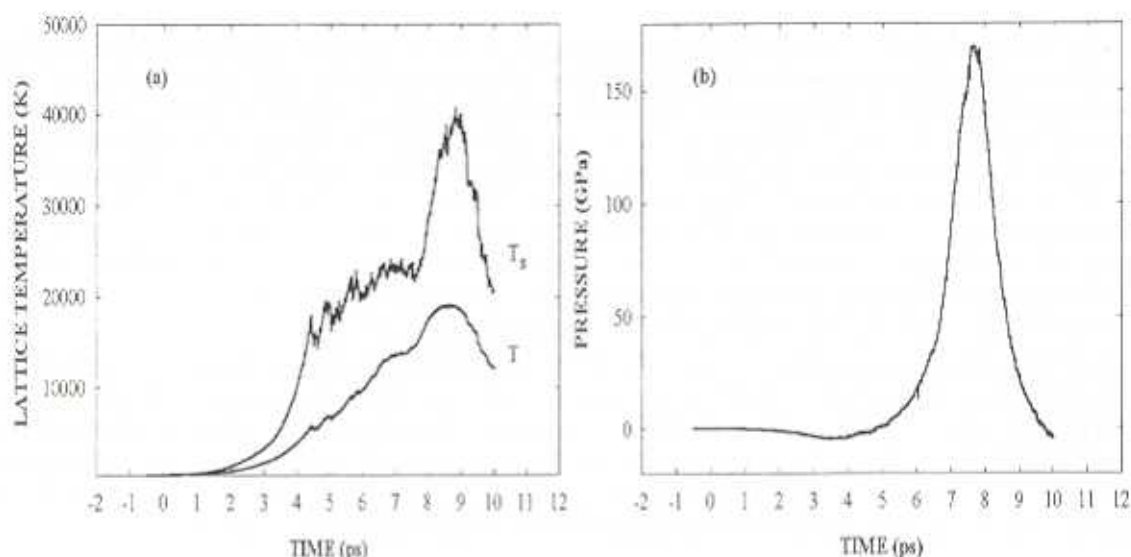
Figure 3. (a) Lattice average (T) and surface (T_s) temperatures vs time. (b) Average pressure vs time. Results are for a single 0.30 J/cm^2 laser pulse where carriers are *not* allowed to diffuse.

As mentioned earlier, the carriers diffuse into the bulk as a consequence of the carrier density gradient at the surface. In order to assess the importance of this mechanism for the relaxation of the system, a simulation for a single 0.30 J/cm^2 pulse was run with the difference that electron-hole pairs were *not* allowed to diffuse following their creation. The carrier-phonon screening effect was also ignored. Fig. 3 shows the lattice-averaged temperature T and the surface temperature T_s in this case. T and T_s reach values of ∼ 18000 K and ∼ 7000 K, respectively, clearly much higher than the experimentally-observed values,[12] which do not exceed ∼ 4000 K at higher fluences. This can be explained by the fact that electron-hole pairs, if not allowed to diffuse, remain within the limits of the supercell in which they release more energy. Furthermore, because carrier diffusion has been suppressed, $T_s > T$ as the maximum temperature is now located *at the surface*.

However, this simulation provides a way to evaluate the importance of carrier diffusion and to gain insight into the mechanisms underlying ablation. Fig. 3 shows the pressure induced in the material: after a sharp build-up of a tensile pressure for the reasons mentioned previously, the system goes into *compression* after approximately 3.5 ps. At the same time, the average coordination at the surface (see Fig. 4) increases to reach a peak of about 5.1 after 3 ps, then drops shortly after a few hundreds of femtoseconds. Finally, the position of the topmost layer, after increasing because of the high tensile pressure, suddenly drops after approximately 4 ps: this reveals a very fast phase transition from solid to gas phase, combined with a high tensile pressure inside the material which causes the sudden removal of atoms from the surface, that is ablation. The pressure then becomes highly compressive as a result of the recoil pressure induced by the expelled atoms.

Fig. 5 shows the total number of atoms removed from the surface, as a function of time. This number undergoes a steep increase at about 4 ps. The composition of the plume is also presented in Fig. 5; only shown are the numbers of single atoms, as well as of Si$_2$, Si$_3$ and Si$_4$ clusters. One can see that *single* atoms are predominant and the number of Si$_n$ clusters rapidly falls as n increases. In fact, though not explicitly shown here, the number of Si$_n$ clusters, for n = 5 and n = 6, is very small, and negligible in the case of Si$_6$ clusters; this in good agreement with recently-published results of von der Linde et al.[12,13]

Thus, when the diffusion of carriers is not taken into account, the resulting lattice surface temperature is much higher than the experimentally-observed values, which do not exceed ∼ 4000 K. Moreover, the carrier density (not shown here) reaches a value of ∼ 10^{23} cm^{-3}, larger than the critical value of 10^{22} cm^{-3} not accounted for in the present model. Finally, ablation is observed after only a few picoseconds, while it is expected to occur on a 10^{-10} s time scale in a regime where thermal processes only are operative. For these reasons, carrier diffusion is believed to
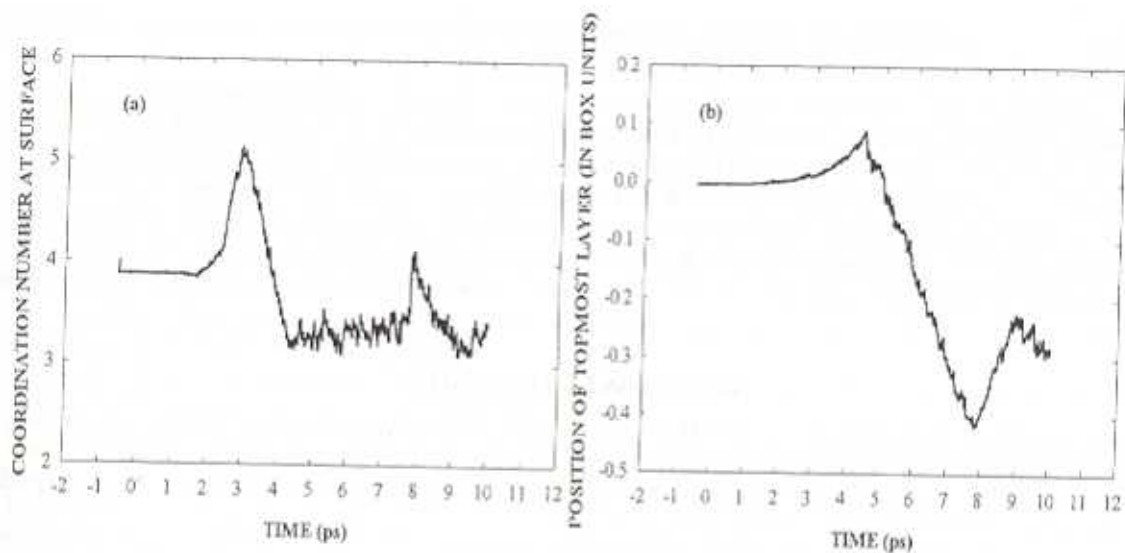
Figure 4. (a) Average coordination number at surface vs time. (b) Position of the surface layer vs time. Results are for a single 0.30 J/cm^2 laser pulse where carriers are *not* allowed to diffuse.
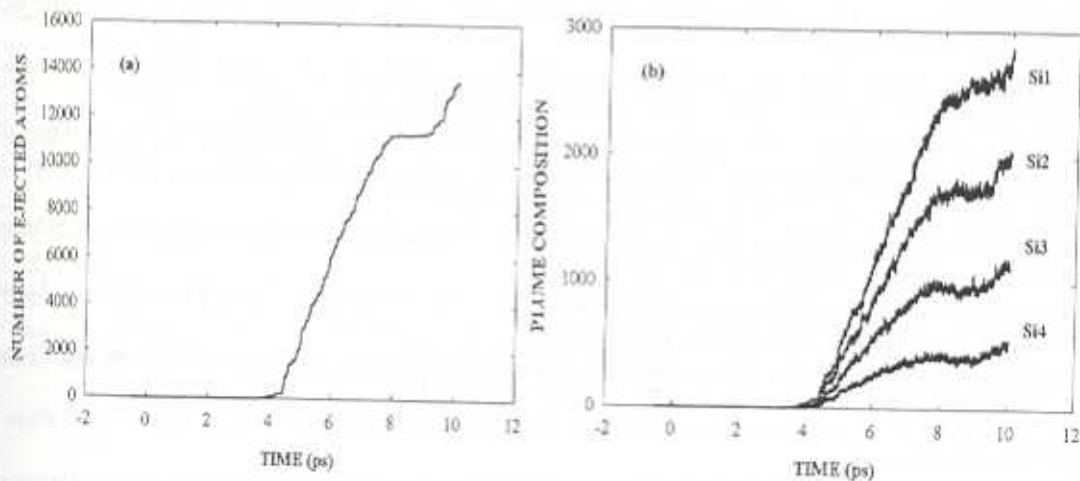

Figure 5. (a) Total number of ejected atoms vs time. (b) Resulting composition of the plume vs time. Results are for a single 0.30 J/cm^2 laser pulse where carriers are *not* allowed to diffuse.

be, in the present context, an essential mechanism for relaxation. These simulations are also helpful in identifying the keys processes that determine the onset and dynamics of laser ablation, namely the laser-induced pressure build-up and the phase explosion due to overheating, as first pointed out by Zhigilei et al.,[5,9] Furthermore, the predicted composition of the plume is in good agreement with recent experimental data.

4. SUMMARY

A molecular-dynamics model has been developed to study the laser ablation of crystalline silicon. All interactions and processes were described within the thermal annealing model. The atoms were chosen to interact at all times through the Stillinger-Weber potential. Simulations involved a system of 32400 atoms of which about 28000 were irradiated by a 308 nm, 10 ps, Gaussian laser pulse. One-photon interband transition is the dominant absorption mechanism.

Carrier-phonon scattering and carrier diffusion into the bulk are taken into account, but Auger recombination and impact ionization are neglected.

Preliminary results were presented. Simulations, when carriers are allowed to diffuse, predict a melting fluence threshold in good agreement with experiment. However, when carrier diffusion is artificially suppressed, incorrect values for the temperature and carrier density are obtained and laser ablation is observed to be unrealistic, occurring in too short a time. For these reasons, carrier diffusion is found to be an essential mechanism for relaxation for the experimental conditions simulated. Furthermore, it is believed to be responsible for the observation of subsurface boiling. Finally, ablation seems to proceed from a high-pressure build-up within the volume combined with a very fast phase transition from solid to gas phase. Full details of the calculations and complete results will be presented elsewhere.

ACKNOWLEDGMENTS

REFERENCES

1. L. L. Chase, "Laser Ablation and Optical Surface Damage," in *Laser ablation: Principles and Applications*, John C. Miller, ed., Springer Series in Materials Science, **25**, Springer-Verlag, Berlin, 1994.
2. R. F. Haglund, Jr., and N. Itoh, "Electronic Processes in Laser Ablation of Semiconductors and Insulators," in *Laser ablation: Principles and Applications*, John C. Miller, ed., Springer Series in Materials Science **28**, Springer-Verlag, Berlin, 1994.
3. R. F. Haglund, Jr., *Laser Ablation and Desorption*, John C. Miller and Richard F. Haglund, Jr., eds., Experimental Methods in the Physical Sciences **30**, Academic Press, San Diego, 1998.
4. D. B. Chrisey and G. K. Hubler, *Pulsed Laser Deposition of Thin Films*, John Wiley and Sons, New-York, 1994.
5. L. V. Zhigilei, P. B. S. Kodali, and B. J. Garrison, "Molecular Dynamics Model for Laser Ablation and Desorption of Organic Solids," *J. Phys. Chem. B* **101**, pp. 2028–2037, 1997.
6. R. F. W. Herrmann, J. Gerlach, and E. E. B. Campbell, "Ultrashort Pulse Laser Ablation of Silicon: an MD Simulation Study," *Appl. Phys. A* **66**, pp. 35–42, 1998.
7. A. Bencsura and A. Vertes, "Dynamics of Hydrogen Bonding and Energy Transfer in Matrix-Assisted Laser Desorption," *Chem. Phys. Lett.* **247**, pp. 142–148, 1995.
8. B. J. Garrison and R. Srinivasan, "Laser Ablation of Organic Polymers: Microscopic Models for Photochemical and Thermal Processes," *J. Appl. Phys.* **57**, pp. 2909–2914, 1985.
9. L. V. Zhigilei, P. B. S. Kodali, and B. J. Garrison, "A Microscopic View of Laser Ablation," *J. Phys. Chem. B* **102**, pp. 2845–2853, 1998.
10. L. V. Zhigilei, P. B. S. Kodali, and B. J. Garrison, "On the Threshold Behavior in Laser Ablation of Organic Solids," *Chem. Phys. Lett.* **276**, pp. 269–273, 1997.
11. F. H. Stillinger and T. A. Weber, "Computer Simulation of Local Order in Condensed Phases of Silicon," *Phys. Rev. B* **31**, pp. 5262–5271, 1985.
12. A. Cavalleri, K. Sokolowski-Tinten, J. Bialkowski, M. Schreiner, and D. von der Linde, "Femtosecond Melting and Ablation of Semiconductors Studied with Time of Flight Mass Spectroscopy," *J. Appl. Phys.* **85**, pp. 3301–3309, 1999.
13. A. Cavalleri, K. Sokolowski-Tinten, J. Bialkowski, and D. von der Linde, "Time of Flight Mass Spectroscopy of Femtosecond Laser Ablation of Solid Surfaces," in *Ultrafast Phenomena* XI, T. Elsaesser, J. G. Fujimoto, D. A. Wiersma and W. Zinth, eds., Springer Series in Chemical Physics **63**, p. 310, Springer, Heidelberg, 1998.
14. D. von der Linde, K. Sokolowski-Tinten, and J. Bialkowski, "Laser-solid Interaction in the Femtosecond Time Regime," *Appl. Surf. Sci.* **109-110**, pp. 1–10, 1997.
15. P. L. Silvestrelli, A. Alavi, M. Parrinello, and D. Frenkel, "*Ab initio* Molecular Dynamics Simulation of Laser Melting of Silicon," *Phys. Rev. Lett.* **77**, pp. 3149–3152, 1996.
16. R. F. Wood and G. E. Jellison, Jr., "Melting Model of Pulsed Laser Processing," in *Pulsed Laser Processing of Semiconductors*, Semiconductors and Semimetals **23**, pp. 166–250, Academic Press, 1984.

17. S. M. Sze, *Physics of Semiconductor Devices*, Wiley-Interscience, New-York, 1969.

18. M. Murayama and T. Nakayama, "Two-Photon-Absorption Spectra Originating from Higher-Energy Transitions," *Phys. Rev. B* **49**, pp. 5737–5740, 1994.

19. A. Lietoila and J. F. Gibbons, "Computer Modeling of the Temperature Rise and Carrier Concentration Induced in Silicon by Nanosecond Laser Pulses," *J. Appl. Phys.* **53**, pp. 3207–3213, 1982.

20. G. E. Jellison, Jr., and F. A. Modine, "Optical Functions of Silicon between 1.7 and 4.7 eV at Elevated Temperatures," *Phys. Rev. B* **27**, pp. 7466–7472, 1983.

21. G. E. Jellison, Jr., and F. A. Modine, "Optical Absorption of Silicon between 1.6 and 4.7 eV at Elevated Temperatures," *Appl. Phys. Lett.* **41**, pp. 180–182, 1982.

22. H. M. van Driel, "Kinetics of High-Density Plasmas Generated in Si by 1.06- and 0.53-μm Picosecond Laser Pulses," *Phys. Rev. B* **35**, pp. 8166–8176, 1987.

23. R. F. Pierret, *Advanced Semiconductor Fundamentals*, Robert F. Pierret and Gerold W. Neudeck, eds., Modular Series on Solid State Devices, vol. VI, Addison-Wesley, 1987.

24. M. Lundstrom, *Fundamentals of Carrier Transport*, Gerold W. Neudeck and Robert F. Pierret, eds., Modular Series on Solid State Devices, vol. X, Addison-Wesley, 1990.

25. M. V. Fischetti and S. E. Laux, "Monte Carlo Analysis of Electron Transport in Small Semiconductor Devices Including Band-Structure and Space-Charge Effects," *Phys. Rev. B* **38**, pp. 9721–9745, 1988.

26. E. J. Yoffa, "Screening of Hot-Carrier Relaxation in Highly Photoexcited Semiconductors," *Phys. Rev. B* **23**, pp. 1909–1919, 1981.

27. P. T. Landsberg, *Recombination in Semiconductors*, Cambridge University Press, Cambridge, 1991.

28. E. J. Yoffa, "Dynamics of Dense Laser-Induced Plasmas," *Phys. Rev. B* **21**, pp. 2415–2425, 1980.

29. F. Berz, R. W. Cooper, and S. Fagg, "Recombination in the End Regions of PIN Diodes," *Solid-State Electron.* **22**, pp. 293–301, 1979.

30. J. R. Goldman and J. A. Prybyla, "Ultrafast Dynamics of Laser-Excited Electron Distributions in Silicon," *Phys. Rev. Lett.* **72**, pp. 1364–1367, 1994.

31. B. Danielzik, P. Harten, K. Sokolowski-Tinten, and D. von der Linde, "Picosecond Laser-Induced Solid-Liquid Phase Transformations in Gallium Arsenide and Silicon," in *Mater. Res. Soc. Symp. Proc.* **100**, pp. 471–476, 1988.

32. N. Bloembergen, "Pulsed Laser Interactions with Condensed Matter," in *Mater. Res. Soc. Symp. Proc.* **51**, pp. 3–13, 1985.

33. K. Sokolowski-Tinten, J. Bialkowski, A. Cavalleri, and D. von der Linde, "Time Resolved Studies of Femtosecond Laser Induced Ablation from Solid Surfaces," in *Ultrafast Phenomena* XI, T. Elsaesser, J. G. Fujimoto, D. A. Wiersma, and W. Zinth, eds., Springer Series in Chemical Physics **63**, pp. 316–318, Springer-Verlag, Heidelberg, 1998.